 CMES, vol.107, no.2, pp.155-186, 2015

Are Higher-Order Theories and Layer-wise Zig-Zag Theories Necessary for N-Layer Composite Laminates?

Qifeng Fan[1], Yaping Zhang[2], Leiting Dong[1,3], Shu Li[1], Satya N. Atluri[4]

Abstract: Although "higher-order" and layer-wise "higher-order" plate and shell theories for composite laminates are widely popularized in the current literature, they involve (1) postulating very complex assumptions of plate/shell kinematics in the thickness direction, (2) defining generalized variables of displacements, strains, and stresses, and (3) developing very complex governing equilibrium, compatibility, and constitutive equations in terms of newly-defined generalized kinemaic and generalized kinetic variables. Their industrial applications are thus hindered by their inherent complexity, and the fact that it is difficult for end-users (front-line structural engineers) to completely understand all the newly-defined FEM DOFs in higher-order and layer-wise theories. In an entirely different way, the authors developed very simple lowest-order (8-node hexahedral), and higher-order (32-node hexahedral) 3-D continuum solid-shell elements, based on the theory of 3D solid mechanics, for static and dynamic analyses of composite laminates. The shear-locking of the lower-order 8-node hexahedral element is alleviated by independently assuming locking-free strain fields for each element. Over-integration is used to evaluate the element stiffness matrices of laminated structures with an arbitrary number of laminae, while only one element is used in the thickness direction without increasing the number of degrees of freedom. A stress-recovery approach is used to compute the distribution of transverse stresses by considering the equations of 3D elasticity. Comprehensive numerical results are presented for static, free vibration, and transient analyses of different laminated plates and shells, which agree well with existing solutions in the published literature, or solutions of very-expensive 3D models (where 3D elements are used to model each layer) by using commercial FEM codes. Because the proposed methodology merely involves simple displacement DOFs at each node, relies only on the simple theory of solid mechanics, and is capable of accurately and efficiently predicting the static

[1] School of Aeronautic Science and Engineering, Beihang University, China
[2] Taizhou Polytechnic College, China
[3] Corresponding Author, Email: dong.leiting@gmail.com
[4] Department of Mechanical Engineering, Texas Tech University, USA

and dynamical behavior of composite laminates in a very simple and cost-effective manner, it is thus believed by the authors that the development of "higher-order" or "layer-wise higher-order" theories are not entirely necessary for analyses of laminated plates and shells.

Keywords: plate, shell, composite laminate, higher order theory, finite element

1 Introduction

Laminated composite structures are extensively used in aerospace, automobile, marine and other industrial fields, primarily due to their high strength-to-mass ratio, high stiffness-to-mass ratio, and their capability to be tailored according to given requirements. In-depth understandings of their mechanical behaviors are generally needed for the design and maintenance of such engineering structures. However, as full or large scale experimental tests are usually time-expensive and monetarily-expensive, it is necessary to develop accurate and efficient numerical models which are capable of predicting their static and dynamical behaviors.

A very large number of laminate theories can be found in the literature, which are mostly derived from equations of 3D elasticity by making various assumptions of the kinematics in the thickness direction. These theories involve expanding the displacement field in a power-series in the thickness direction of the entire laminate (classic, first-order and higher-order theories) or in the thickness direction of each lamina in the laminate (layer-wise higher-order theories). Using these assumptions, a new set of generalized displacements, strains, and stresses are defined, and a new set of governing equilibrium, compatibility, and constitutive equations are derived. The simplest one is the classical laminate theory (CLT) which is based on the well-known Love-Kirchoff assumption [Timoshenko and Woinowsky (1959)]. Straight lines normal to the mid-surface are assumed to remain straight and normal to the mid-surface after deformation. To take into account the effects of transverse shear deformation, the first-order shear deformation theory (FSDT) [Reissner (1945) and Mindlin (1951)] relaxes the Love-Kirchoff assumption, so that transverse straight lines do not necessarily remain normal to the mid-surface after deformation [see Fig. 1(a)]. CLT and FSDT are widely popularized in commercial FEM packages such as Ansys, Abaqus, Nastran, etc. But for very thick composite laminates, CLT and FSDT usually underestimate the deflections and overestimates natural frequencies.

Many higher-order shear deformation theories (HSDT) were later proposed, see [Lo, Christensen and Wu (1977); Reddy (1984); Pandya and Kant (1988); Reddy and Robbins (1994)]. These high-order theories mostly adapt various third-order assumptions of in-plane displacements [see Fig. 1(b)], define additional general-

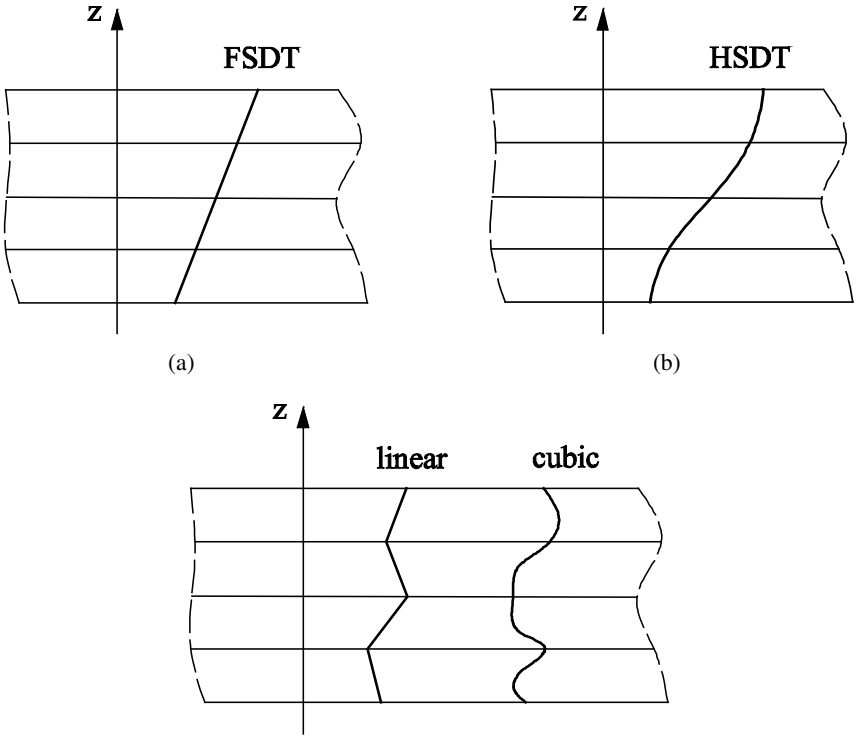

Figure 1: Assumptions of kinematics in the thickness direction composite laminates by (a) first order shear deformation theory (FSDT), (b) higher order shear deformation theory (HSDT), (c) layer-wise higher-order theories

ized variables that have ambiguous physical meanings, and derive very complex and tedious governing differential equations of plate and shells. For example, Lo, Christensen and Wu (1977) postulated the following expansion of displacements in the thickness direction:

$$\begin{aligned} u &= u_0 + z\phi_x + z^2\varphi_x + z^3\theta_x \\ v &= v_0 + z\phi_y + z^2\varphi_y + z^3\theta_y \\ w &= w_0 + z\phi_z + z^2\varphi_z \end{aligned} \tag{1}$$

where $\varphi_x, \varphi_y, \varphi_z, \theta_x, \theta_y$ are often referred as "higher-order rotations" which specify the deformed shapes of straight lines normal to the mid-surface of unreformed plates and shells. Based on Eq. (1), Reddy (1984) further derived the following assumption of displacements in the thickness direction, by enforcing the vanishing

of transverse shear stresses at the top and bottom surfaces of plates and shells.

$$
\begin{aligned}
u &= u_0 + z\phi_x - z^2\left(\frac{1}{2}\frac{\partial \phi_z}{\partial x}\right) - z^3\left[\frac{4}{3h^2}\left(\frac{\partial w_0}{\partial x} + \phi_x\right) + \frac{1}{3}\frac{\partial \varphi_z}{\partial x}\right] \\
v &= v_0 + z\phi_y - z^2\left(\frac{1}{2}\frac{\partial \phi_z}{\partial y}\right) - z^3\left[\frac{4}{3h^2}\left(\frac{\partial w_0}{\partial y} + \phi_y\right) + \frac{1}{3}\frac{\partial \varphi_z}{\partial y}\right] \\
w &= w_0 + z\phi_z + z^2\varphi_z
\end{aligned}
\tag{2}
$$

However, one can easily see that, if one is to develop finite elements based on Eq. (1), only C^0 continuous interpolations are needed. But C^1 continuous interpolations are needed for Reddy's third order theory based on Eq. (2), which are not practical for general-purpose finite element implementations.

In a similar way the layer-wise theories are developed by making assumptions of displacements in each layer, see [Swift and Heller (1974); Seide (1980); Reddy (1984); Di Sciuva (1985); Carrera (2003)]. Displacements in each layer or lamina are assumed to be either linear, quadratic, higher-order, trigonometric, or to be other continuous functions in layer-wise/zig-zag theories of plates and shells [see Fig. 1(c)]. However, having additional degrees of freedoms for each lamina makes layer-wise theories highly expensive for realistic laminate structures that have a very large number of layers. For example, [Reddy (1984)] expresses displacements in the k^{th} layer of the laminate as:

$$
\begin{aligned}
u^k &= \sum_i u_i^k \phi_i^k \\
v^k &= \sum_i v_i^k \phi_i^k \\
w^k &= \sum_i w_i^k \phi_i^k
\end{aligned}
\tag{3}
$$

In order to derive higher-order or layer-wise theories of plates and shells, kinematic assumptions are substituted into the principle of potential energy of 3D elasticity. By exploring the stationarity conditions, very complex governing differential equations in terms of newly defined generalized displacements, strains and stresses can be derived, see [Reddy (2004)] for example. However, such complex differential equations cannot be directly solved. One usually goes back to derive a variational principle from these governing differential equations, and to develop corresponding finite element models to solve the problem numerically. In this sense, defining the many generalized displacements, strains, stresses, and deriving the complex higher-order or layer-wise theories and differential equations seems unnecessary. One can directly use the variational principle of 3D elasticity to develop finite elements for the modeling of plates and shells. Moreover, it is difficult for end-users

to completely understand all the newly-defined FEM DOFs in higher-order theories which have ambiguous physical meanings, which becomes very problematic when boundary conditions have to be enforced correctly by end-users.

In an entirely different way, [Dong, El-Gizawy, Juhany, Atluri (2014b, c)] directly developed quadrilateral 4-node, and hexahedral 8-node finite element models, for FG and laminated structures based on the theory of 2-D and 3-D solid mechanics, respectively. Because traditional displacement-based lowest order elements suffer from shear locking, a technique of locking-alleviation was used by independently assuming locking-free element strains. Over-integration was also adapted in the thickness direction to accurately evaluate the stiffness matrix of FG and laminated elements. Similar work on smart composite structures was also presented in [Ray, Dong and Atluri (2015)]. However, for very thick laminated structures with only a few layers, the computational accuracy is slightly compromised if only one linear finite element is used in the thickness direction. [Fan, Zhang, Dong, Li, Atluri (2015)] further developed very simple displacement-based 32-node hexahedral element for static and dynamic analyses of composite laminates. And a stress-recovery approach was used to compute the distribution of transverse stresses by considering the equations of 3D elasticity.

In this study, comprehensive numerical results are presented for static, free vibration, and transient analyses of different laminated plates and shells, which agree well with existing solutions in the published literature, or solutions of very-expensive 3D models by commercial FEM codes. Because the proposed methodology merely involves displacement DOFs at each node, relies only on the simple theory of solid mechanics, and is capable of accurately and efficiently predicting the static and dynamical behavior of composite laminates in a very simple and cost-effective manner, it is thus believed by the authors that the development of higher-order or layer-wise theories are not entirely necessary for analyses of laminated plates and shell. In the following sections, details of the proposed methodology are described and numerical examples of various laminated plates/shells with different loads and boundary conditions are provided.

2 Formulations of the Present Simple Elements

As illustrated in Fig. 2, nodal shape functions of the 8-node, 20-node and 32-node hexahedral elements can defined in terms of local isoperimetric coordinates, which can be found in most books of finite elements [Atluri (2005), Zienkiewicz and Taylor (1997)]. For example, shape functions of the 8-node hexahedral element are as follows:

$$N^{(1)} = (1-\xi)(1-\eta)(1-\varsigma)/8$$

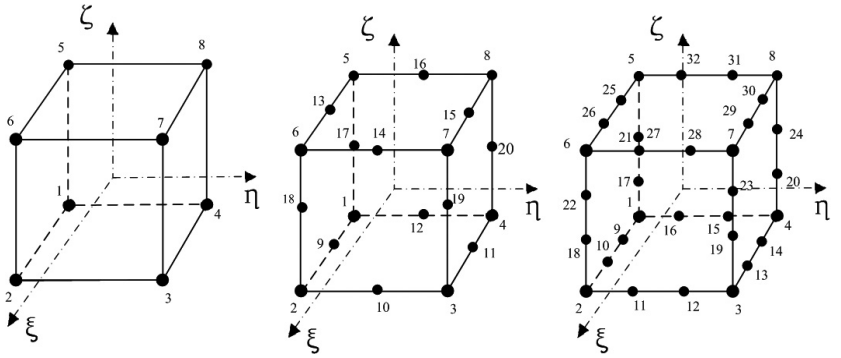

Figure 2: Topologies of the 8-node, the 20-node, and the 32-node hexahedral elements

$$
\begin{aligned}
N^{(2)} &= (1+\xi)(1-\eta)(1-\varsigma)/8 \\
N^{(3)} &= (1+\xi)(1+\eta)(1-\varsigma)/8 \\
N^{(4)} &= (1-\xi)(1+\eta)(1-\varsigma)/8 \\
N^{(5)} &= (1-\xi)(1-\eta)(1+\varsigma)/8 \\
N^{(6)} &= (1+\xi)(1-\eta)(1+\varsigma)/8 \\
N^{(7)} &= (1+\xi)(1+\eta)(1+\varsigma)/8 \\
N^{(8)} &= (1-\xi)(1+\eta)(1+\varsigma)/8.
\end{aligned} \tag{4}
$$

And displacement fields within the element are interpolated by using nodal shape functions:

$$u_i = \sum_I N^{(I)} \tilde{u}_i^{(I)} \tag{5}$$

or in equivalent matrix-vector notations:

$$\mathbf{u} = \mathbf{N}\tilde{\mathbf{u}}^e \tag{6}$$

where $\tilde{\mathbf{u}}^e$ represents nodal displacements of the element.

Traditional displacement-based primal finite elements determine the strain fields within the element by differentiating Eq. (6) with respect to Cartesian coordinates:

$$\boldsymbol{\varepsilon} = \mathbf{L}\mathbf{u} = \mathbf{L}\mathbf{N}\tilde{\mathbf{u}}^e = \mathbf{B}\tilde{\mathbf{u}}^e \tag{7}$$

where $\mathbf{L}$ is a linear differential operator.

By using the Galerkin Weak-Form or equivalent variational principles [Atluri (2005)], the element stiffness matrix and mass matrix are computed by:

$$\begin{aligned} \mathbf{k}^e &= \int_{\Omega^e} \mathbf{B}^{\mathbf{T}}\mathbf{D}\mathbf{B} d\Omega \\ \mathbf{m}^e &= \int_{\Omega^e} \mathbf{N}^{\mathbf{T}}\rho\mathbf{N} d\Omega. \end{aligned} \tag{8}$$

We thus denote displacement-based primal 8-node, 20-node, and 32-node finite elements developed following the algorithms described above as DPH8, DPH20, and DPH32 respectively. However, as discussed in [Atluri (2005); Dong and Atluri (2011)], lowest-order hexahedral element DPH8 surfer from shear locking, which will be problematic when being used to model thin structures such as plates and shell. This is due to that interpolated displacement fields of DPH8 are incomplete, so that bending strains derived from interpolated displacements are locked to shear strains. A locking-alleviation technique was thus developed in [Dong, El-Gizawy, Juhany, Atluri (2014c)], by independently assuming a locking-free 18-parameter linearly-varying strain field within the element, which can be rewritten in a matrix-vector notation for convenience:

$$\boldsymbol{\varepsilon}^* = \mathbf{A}\boldsymbol{\gamma} \tag{9}$$

where $\boldsymbol{\gamma}$ represents undetermined 18 parameters of the assumed linear strain field. By exactly enforcing 18 pre-defined constraints at 18 pre-selected collocation points, the 18 parameters are related to nodal displacements as:

$$\boldsymbol{\gamma} = \mathbf{C}\tilde{\mathbf{u}}^e. \tag{10}$$

And thus the strain fields within the element are reconstructed as:

$$\boldsymbol{\varepsilon}^* = \mathbf{A}\mathbf{C}\tilde{\mathbf{u}}^e = \mathbf{B}^*\tilde{\mathbf{u}}^e \tag{11}$$

which are inherently lock-free as is defined from the beginning.

And the element stiffness matrix is determined from the strain energy stored in the element:

$$\mathbf{k}^{\mathbf{e}} = \int_{\Omega^e} \mathbf{B}^{*T}\mathbf{D}\mathbf{B}^* d\Omega \tag{12}$$

Following the denotation of [Dong, El-Gizawy, Juhany, Atluri (2014c)], we call this locking-free 8-node hexahedral element as CEH8. As discussed in [Dong,

EI-Gizawy, Juhany and Atluri (2014b, c)], the technique of "over integration" is needed to accurately evaluate the element stiffness and mass matrices of CEH8, DPH20, and DPH32 when they are used to model laminated structures. In order to take care of the different material properties of each lamina, a layer-wise Gauss quadrature in the thickness direction is adapted. In this way, we consider another variable ς_k as the natural coordinate in the thickness direction of any (k^{th}) individual layer, which can be related to the natural coordinate ς of the whole element in the thickness direction as follows:

$$\varsigma = \frac{1}{h}(h_k + h_{k+1}) + \frac{\varsigma_k}{h}(h_{k+1} - h_k) \tag{13}$$

where h, h^k, h^{k+1} represent the thickness of the plate/shell, and coordinates in the thickness direction at the bottom and the top surfaces of any layer of lamina.

Thus the elemental stiffness and mass matrix are to be evaluated as:

$$\begin{aligned}
k^e &= \int_{-1}^{1}\int_{-1}^{1}\sum_{k=1}^{N}\int_{-1}^{1} B^{*T} D_k B^* |J| \frac{(h_{k+1}-h_k)}{h} d\varsigma_k d\xi d\eta \quad \text{(for CEH8)} \\
k^e &= \int_{-1}^{1}\int_{-1}^{1}\sum_{k=1}^{N}\int_{-1}^{1} B^{T} D_k B |J| \frac{(h_{k+1}-h_k)}{h} d\varsigma_k d\xi d\eta \quad \text{(for DPH20 and DPH32)} \\
m^e &= \int_{-1}^{1}\int_{-1}^{1}\sum_{k=1}^{N}\int_{-1}^{1} N^{T} \rho_k N |J| \frac{(h_{k+1}-h_k)}{h} d\varsigma_k d\xi d\eta
\end{aligned} \tag{14}$$

where D_k and ρ_k are elastic stiffness and density of the k^{th} layer respectively.

The transverse normal and shear stresses are computed by using a stress-recovery approach considering the equilibrium equations of 3D linear elasticity. For the laminated plates, the distribution of transverse stresses can be obtained by numerically evaluating:

$$\begin{aligned}
\sigma_{zx} &= -\int_{z_0}^{z} (\sigma_{xx,x} + \sigma_{xy,y}) dz \\
\sigma_{zy} &= -\int_{z_0}^{z} (\sigma_{yy,y} + \sigma_{xy,x}) dz \\
\sigma_{zz} &= -\int_{z_0}^{z} (\sigma_{zx,x} + \sigma_{zy,y}) dz
\end{aligned} \tag{15}$$

where $z = z_0$ denote the lower surface of the plate.

For cylindrical shells, the distribution of transverse stresses can also be evaluated, by numerically solving the following 3 differential equations:

$$\begin{aligned}
&\frac{\partial \sigma_{r\theta}}{\partial r}+2\frac{\sigma_{r\theta}}{r}=-\frac{1}{r}\frac{\partial \sigma_{\theta\theta}}{\partial \theta}-\frac{\partial \sigma_{\theta z}}{\partial z}\\
&\frac{\partial \sigma_{rz}}{\partial r}+\frac{\sigma_{rz}}{r}=-\frac{\partial \sigma_{zz}}{\partial z}-\frac{1}{r}\frac{\partial \sigma_{\theta z}}{\partial \theta}\\
&\frac{\partial \sigma_{rr}}{\partial r}+\frac{\sigma_{rr}}{r}=\frac{\sigma_{\theta\theta}}{r}-\frac{1}{r}\frac{\partial \sigma_{r\theta}}{\partial \theta}-\frac{\partial \sigma_{rz}}{\partial z}
\end{aligned} \tag{16}$$

In Eq. (16), the left hand-side involves stress components to be recovered, and the right-hand side is directly evaluated from the solutions of finite elements. Each equation is a first-order single-variable ODE, which can be solved with a variety of computational methods, see [Dong, Alotaibi, Mohiuddine and Atluri (2014a)]. In this study, simple collocation of Eq. (16) is implemented at a variety of points along the thickness direction. Combined with the traction free condition at the inner surface of the cylindrical shell, stress components $\sigma_{r\theta}, \sigma_{rz}, \sigma_{rr}$ can be efficiently recovered from the computed in-plane normal and shear stresses.

It should be noted that, through a large number numerical results, the authors find out that DPH20 gives very similar results to CEH8, while DPH32 gives slightly better results as compared to CEH8, with a price of higher computational costs. Thus, in the follow section, only numerical results for CEH8 and DPH32 are given, while results for DPH20 are omitted.

3 Numerical Examples

In this section, several typical problems of laminated composite plates and shells have been analyzed. The geometry and reference system for the laminated plate and shell can be seen in Fig. 3 and Fig. 4 respectively. The following boundary conditions have been used.

Simply supported boundary condition (S):

$\sigma_x = v = \omega = 0$ at $x = 0, a$

$\sigma_y = u = \omega = 0$ at $y = 0, b$

Clamped boundary condition (C)

$u = v = \omega = 0$ at $x = 0, a$ and $y = 0, b$

Free boundary condition (F)

u, v and ω free at $x = 0, a$ and $y = 0, b$

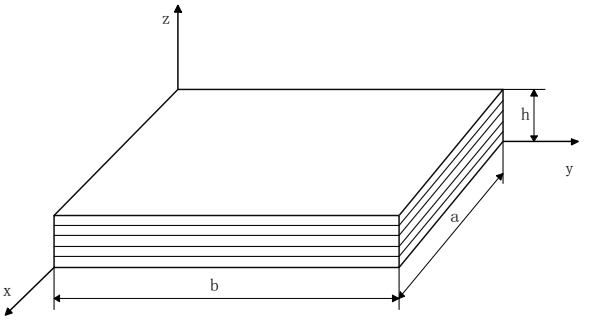

Figure 3: Geometry and reference system for the laminated plate.

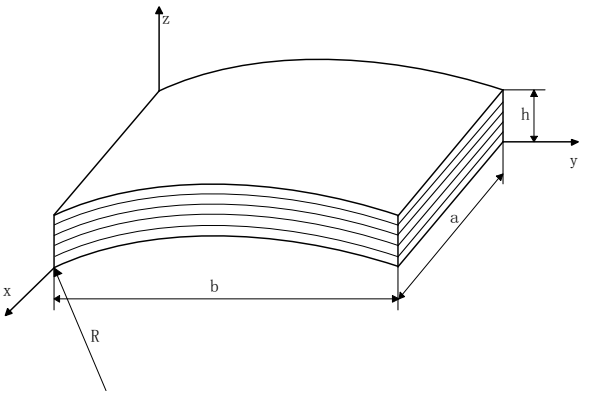

Figure 4: Geometry and reference system for the laminated shell.

3.1 Static analysis

3.1.1 A simply-supported 4-ply ([0/90]$_s$) laminated plate subjected to a sinusoidal distributed lateral load

The first example considers a simply-supported thick-section symmetrical 4-ply ([0/90]$_s$) laminated plate subjected to a sinusoidal distributed lateral load:

$$q = \sin(\pi\frac{x}{a})\sin(\pi\frac{x}{b}).$$

The plate is square with $a = b = 100$ mm, and the total plate thickness is $h = 10$ mm. Each layer is made of Graphite-Epoxy T300/934 with the same thickness. The orthotropic material has the following mechanical properties:

$$E_1 = 131 \text{ GPa}, E_2 = E_3 = 10.34 \text{ GPa},$$

$$G_{12} = G_{13} = 6.895 \text{ GPa}, G_{23} = 6.205 \text{ GPa},$$

$$v_{12} = v_{13} = 0.22, v_{23} = 0.49, \rho = 1627 \text{ kg/m}^3.$$

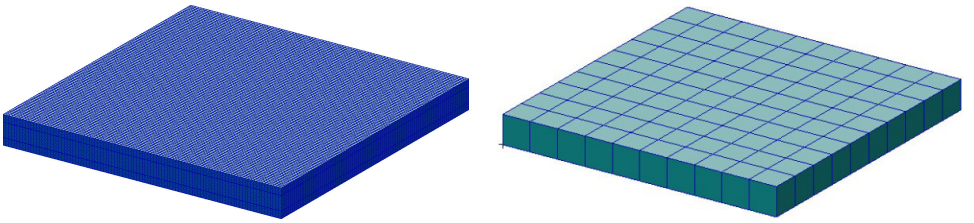

(a) (b)

Figure 5: Finite element model for the 4-ply laminated plate ($a/h = 10$) by (a) Nastran and (b) present CEH8 and DPH32 elements.

We solve this problem using a uniform 10×10 mesh with CEH8 and DPH32 elements, as well as using Nastran by meshing each layer of the laminate. We can see the difference of meshes between the Nastran model and the CEH8/DPH32 model in Fig 4. It takes about half an hour to obtain the numerical results by using the 200,000 nodes Nastran model on a regular PC with i7 CPU. On the contrary, the DPH32 model has only 1364 nodes and takes about 20 seconds of computational time, and the CEH8 model has only 242 nodes and takes about 5 seconds of computational time, although an un-optimized MatLab code is used in this study. Computed in-plane and out-of-plane stresses are shown in Figs. 6–8, from which we can see that the three methods give similar results, although the computation time of Nastran are larger by two orders of magnitudes. The computational accuracy of DPH32 is slightly better than that of CEH8, with a price of larger computational time.

3.1.2 A simply-supported 50-ply ($[0/90]_{25}$) laminated plate subjected to a uniform lateral load

In this subsection, we consider a thick-section unsymmetrical 50-ply ($[0/90]_{25}$) laminated plate. The plate is square with $a = b = 10$ inches, and the thickness of the plate is $h = 1$ inch. The material parameters are as follows:

$E_L = 25 \times 10^6$ psi,$E_T = 1 \times 10^6$ psi,
$G_{LL} = 0.5 \times 10^6$ psi,$G_{LT} = 0.2 \times 10^6$ psi,
$v_{LT} = 0.25, v_{TT} = 0.25,$

where L denotes the fiber's direction and T denotes the transverse direction.

The laminated plate is simply-supported at each edge. And it is subjected to a uniform lateral load $q = 1$ psi.

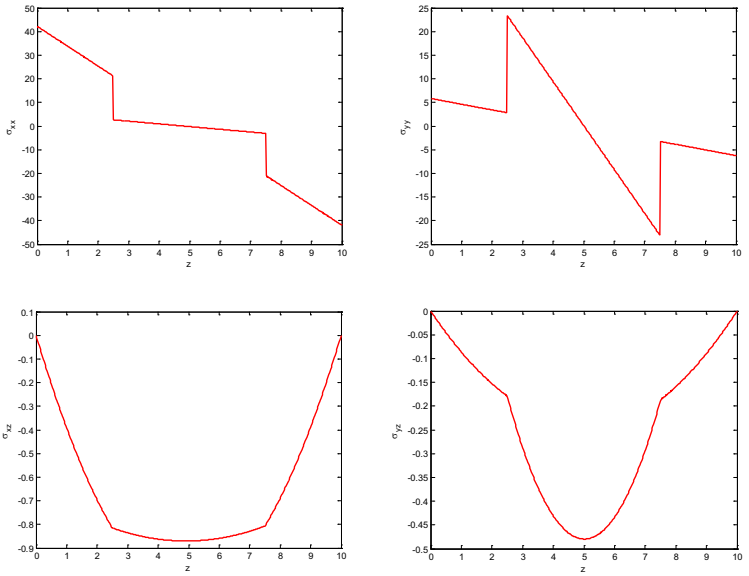

Figure 6: Computed σ_{xx}, σ_{yy} at $x = y = 45$ mm, and computed σ_{xz}, σ_{yz} at $x = y = 10$ mm, for the symmetrical 4-ply thick-section laminated plate ($a/h = 10$), with CEH8.

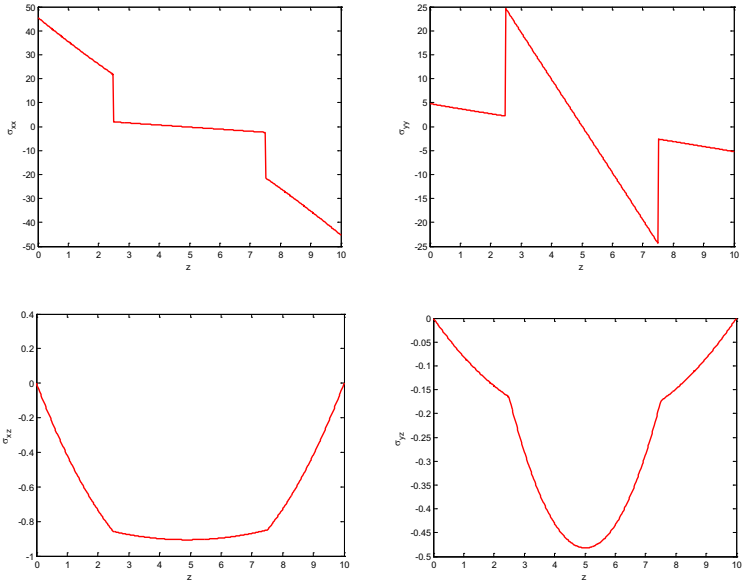

Figure 7: Computed σ_{xx}, σ_{yy} at $x = y = 45$ mm, and computed σ_{xz}, σ_{yz} at $x = y = 10$ mm, for the symmetrical 4-ply thick-section laminated plate ($a/h = 10$), with DPH32.

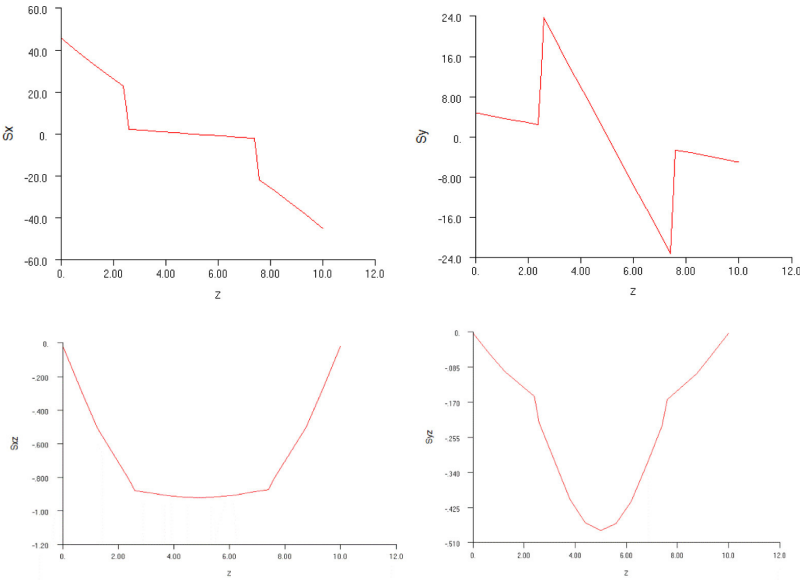

Figure 8: Computed σ_{xx}, σ_{yy} at $x = y = 45$ mm, and computed σ_{xz}, σ_{yz} at $x = y = 10$ mm, for the symmetrical 4-ply thick-section laminated plate ($a/h = 10$), with Nastran.

We solve this problem using a uniform 10×10 mesh with CEH8 and DPH32 elements. Computed in-plane and out-of-plane stresses by present DPH32 elements and Nastran are shown in Figs. 9–10. It is observed that the present CEH8 and DPH32 solutions agree well with the Nastran solutions. *Because of the necessity of meshing each of the 50 layers of laminae for Nastran, it takes about 2.5 hours of computational time and about 1.5 million DOFs in Nastran.* However, the present DPH32 only requires 1364 nodes and about 20 seconds of computational time, and the present CEH8 only requires 242 nodes and about 5 seconds of computational time. One can further observe that, in contrast to the last example of 4-layer thick laminate, CEH8 and DPH32 give almost the same computational results for this 50-layer thick laminate. Since thick laminates applied in aerospace, automobile, marine and other industrial fields usually have a large number of layers, CEH8 should suffice in static analyses such laminated plates and shells.

A different plate with a very-high aspect ratio is also considered in this subsection. The same material properties, the same 50-ply ($[0/90]_{25}$) laminate, and the same boundary conditions and loads are adopted. However, the laminated plate has an aspect ratio of 1000 with $a = b = 1000$ inches and $h = 1$ inch. We also solve this problem with 10×10 CEH8 and 10×10 DPH32 elements. The computed stresses by DPH32 and by CEH8 elements [Dong, El-Gizawy, Juhany and Atluri (2014b)]

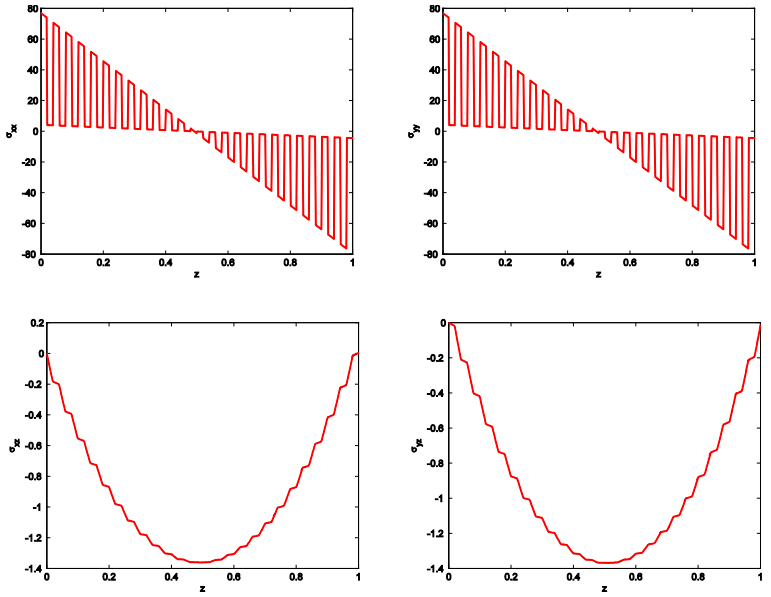

Figure 9: Computed σ_{xx}, σ_{yy} at $x = y = 4.5$ inches, and computed σ_{xz}, σ_{yz} at $x = y = 1$ inch, for the unsymmetrical 50-ply thick-section laminated plate ($a/h = 10$), with CEH8.

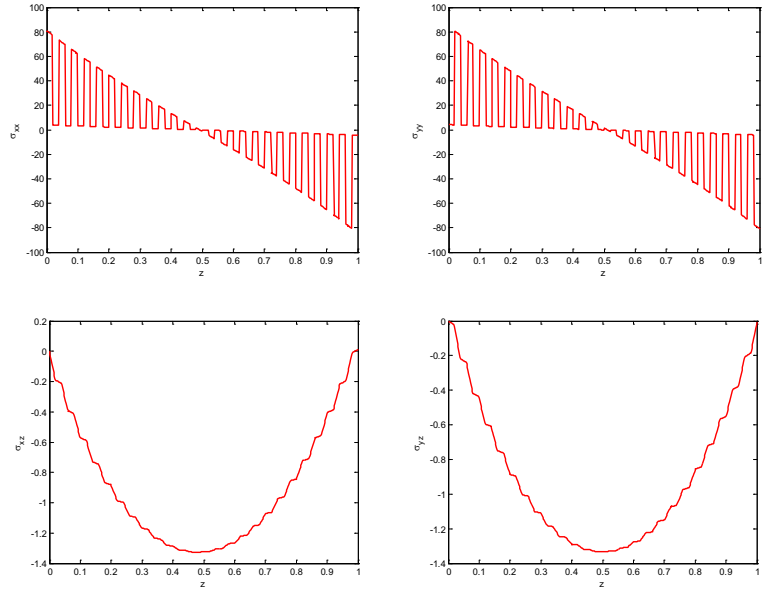

Figure 10: Computed σ_{xx}, σ_{yy} at $x = y = 4.5$ inches, and computed σ_{xz}, σ_{yz} at $x = y = 1$ inch, for the unsymmetrical 50-ply thick-section laminated plate ($a/h = 10$), with DPH32.

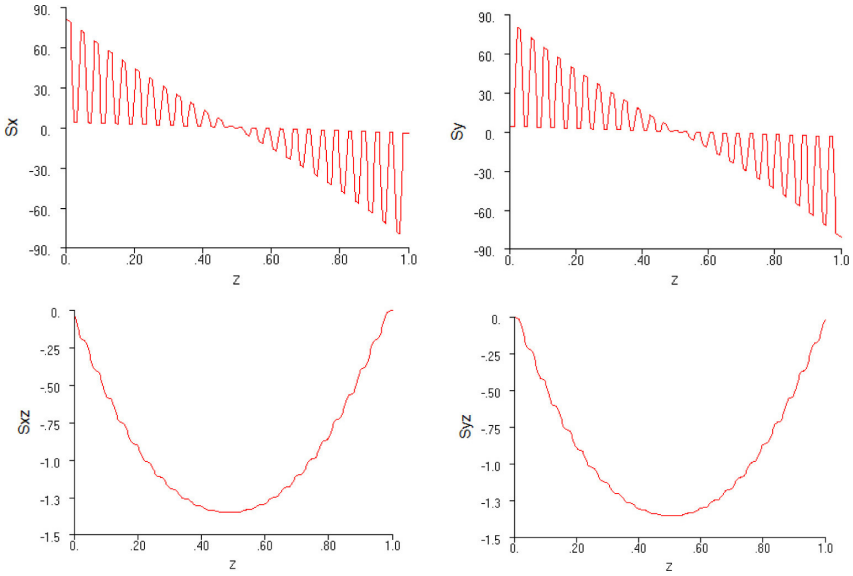

Figure 11: Computed σ_{xx}, σ_{yy} at $x = y = 4.5$ inches, and computed σ_{xz}, σ_{yz} at $x = y = 1$ inch, for the unsymmetrical 50-ply thick-section laminated plate ($a/h = 10$), with Nastran

are shown in Figs. 12–13. Very good agreement is observed. This demonstrates that the present method can deal with the problems of both thick and thin plates, without having to resorting to theories of plates and shells.

3.2 Free vibration analysis

3.2.1 Modal analysis of a thick-section 10-ply [0/90]$_5$laminated square plate

The free vibration of a thick-section 10-ply ($[0^\circ/90^\circ]_5$) laminated plate is analyzed in this subsection. The plate is square with $a = b = 100$ mm, and the thickness is $h = 10$ mm. The material properties are the same as those in the first example. Four different boundary conditions (BCs) are enforced. They are SSSS (simply supported at each edge), CFFF (clamped at $x = 0$ and free at $x = a, y = 0, b$), CSCS (clamped at $x = 0, a$ and simply supported at $y = 0, b$) and CSFS (clamped at $x = 0$, free at $x = a$, and simply supported at $y = 0, b$).

We solve these problems using a uniform 10×10 mesh with CEH8 and DPH32 elements, as well as using Nastran. Comparison between the meshes of the DPH32 model and the Nastran model is given in Fig 14. The non-dimensional frequencies $\overline{\omega}_n = \omega_n a^2/h\sqrt{\rho/E_2}$ are used for comparison of numerical results. The first six mode shapes, for each case, are depicted in Figs. 15–17 in which the corre-

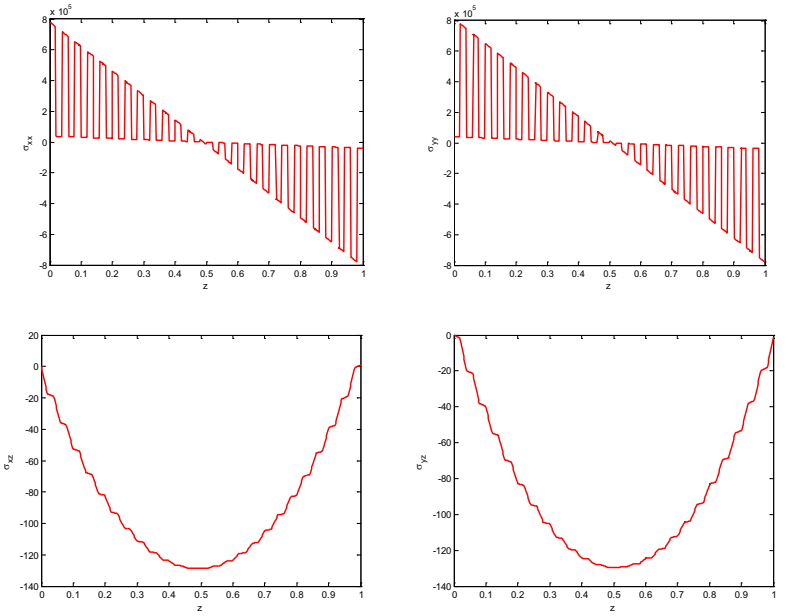

Figure 12: Computed σ_{xx}, σ_{yy} at $x = y = 450$ inches, and computed σ_{xz}, σ_{yz} at $x = y = 100$ inches, for the thin-section laminated plate ($a/h = 1000$), with DPH32.

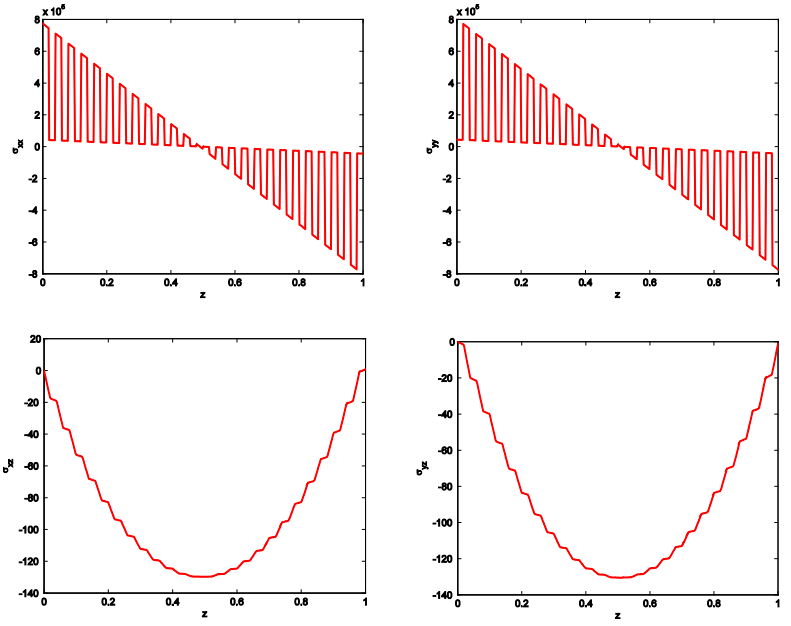

Figure 13: Computed σ_{xx}, σ_{yy} at $x = y = 450$ inches, and computed σ_{xz}, σ_{yz} at $x = y = 100$ inches, for the thin-section laminated plate ($a/h = 1000$), with CEH8.

spondent non-dimensional frequency is reported below each mode shape within the reference Nastran solution. Since the mode shapes computed by CEH8 and DPH32 are so similar, only mode shaped computed by DPH32 are demonstrated. As can be seen from the results, the difference of the frequency parameters between DPH32 and Nastran does not exceed 0.57% for the worst case, and the difference of the frequency parameters between CEH8 and Nastran does not exceed 4.02% for the worst case,. In the meantime, the present DPH32 elements require about 200 times less computational time as compared to Nastran.

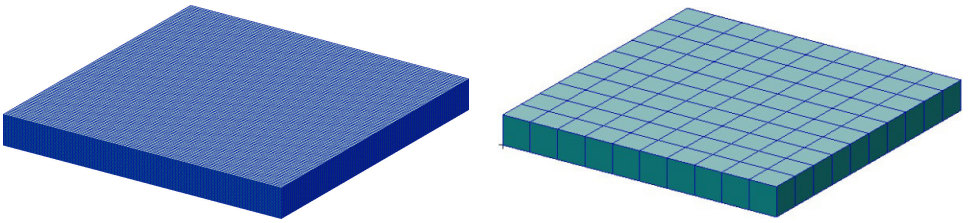

(a) (b)

Figure 14: Finite element model for the 10-ply laminated plate ($a/h = 10$) by (a) Nastran with 400,000 elements and (b) present CEH8/DPH32 with 100 elements.

3.2.2 Modal analysis a thick-section 10-ply [0/90]$_5$laminated shell

In this subsection, we consider a thick-section 10-ply ($[0^\circ/90^\circ]_5$) laminated shell. Each layer of the laminate is composed of the same Graphite–Epoxy T300/934 material whose material parameters are given in the first example. The depth and thickness of the cylindrical shell are $a = 100$ mm and $h = 10$ mm respectively. The arc length of the shell is 100 mm and its corresponding angular span is $\pi/3$. We investigate four different boundary conditions which are SSSS (simply supported at each edge), CFFF (clamped at $x = 0$ and free at $x = a, y = 0, b$), CSCS (clamped at $x = 0, a$ and simply supported at $y = 0, b$) and CSFS (clamped at $x = 0$, free at $x = a$, and simply supported at $y = 0, b$).

We solve these problems using a uniform 10×10 mesh with CEH8 and DPH32 elements, as well as using Nastran. Comparison between the meshes by present elements and by Nastran is given in Fig 19. Computed non-dimensional frequencies and corresponding mode shapes by CEH8/DPH32 and Nastran are given in Figs. 20–24 respectively. Very good agreement is observed for all the results. The difference of the non-dimensional frequencies does not exceed 0.60% for the worst case, and the difference of the frequency parameters between CEH8 and Nastran does not exceed 3.20% for the worst case.

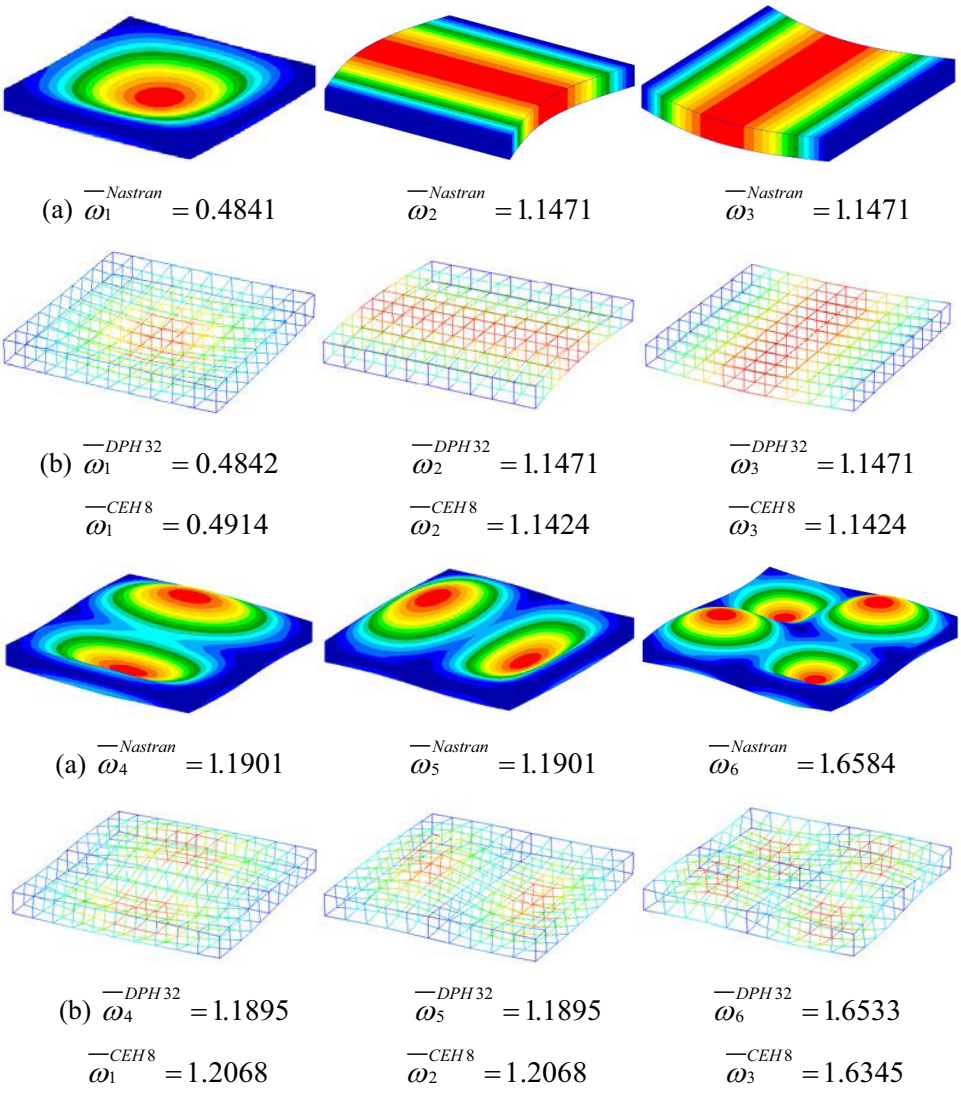

Figure 15: First six non-dimensional frequency parameters and their corresponding mode shapes of a SSSS square laminated plate by (a) Nastran and (b) present CEH8 and DPH32 elements.

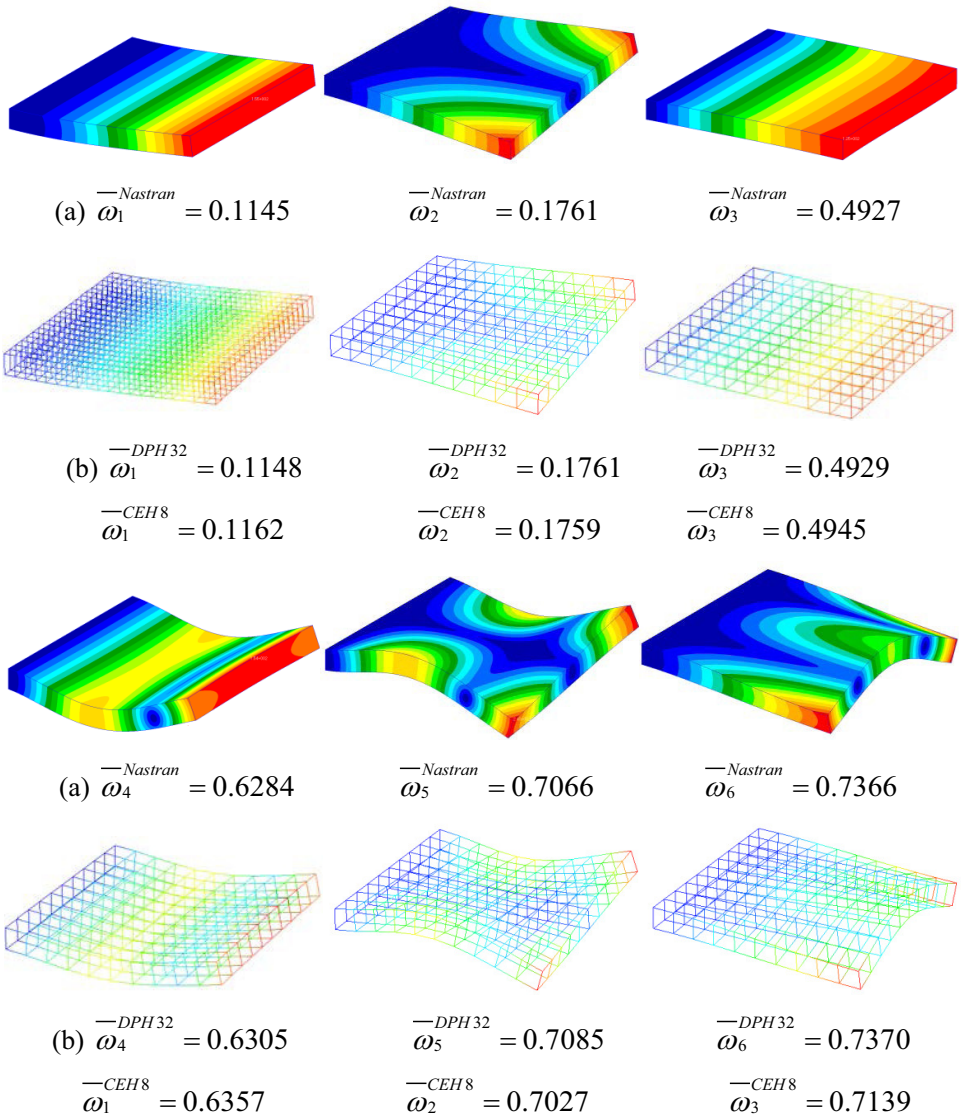

Figure 16: First six non-dimensional frequency parameters and their corresponding mode shapes of a CFFF Square laminated plate by (a) Nastran and (b) present CEH8 and DPH32 elements.

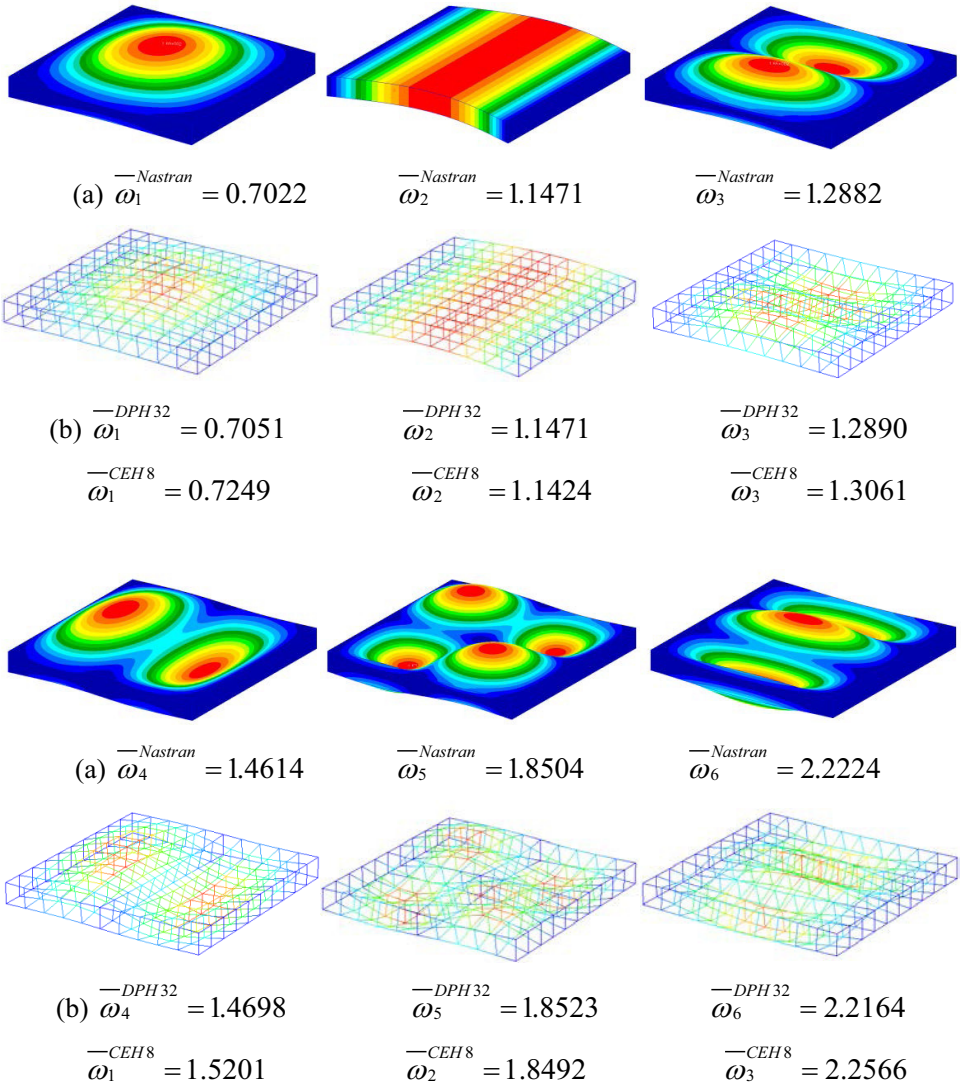

Figure 17: First six non-dimensional frequency parameters and their corresponding mode shapes of a CSCS Square laminated plate by (a) Nastran and (b) present CEH8 and DPH32 elements.

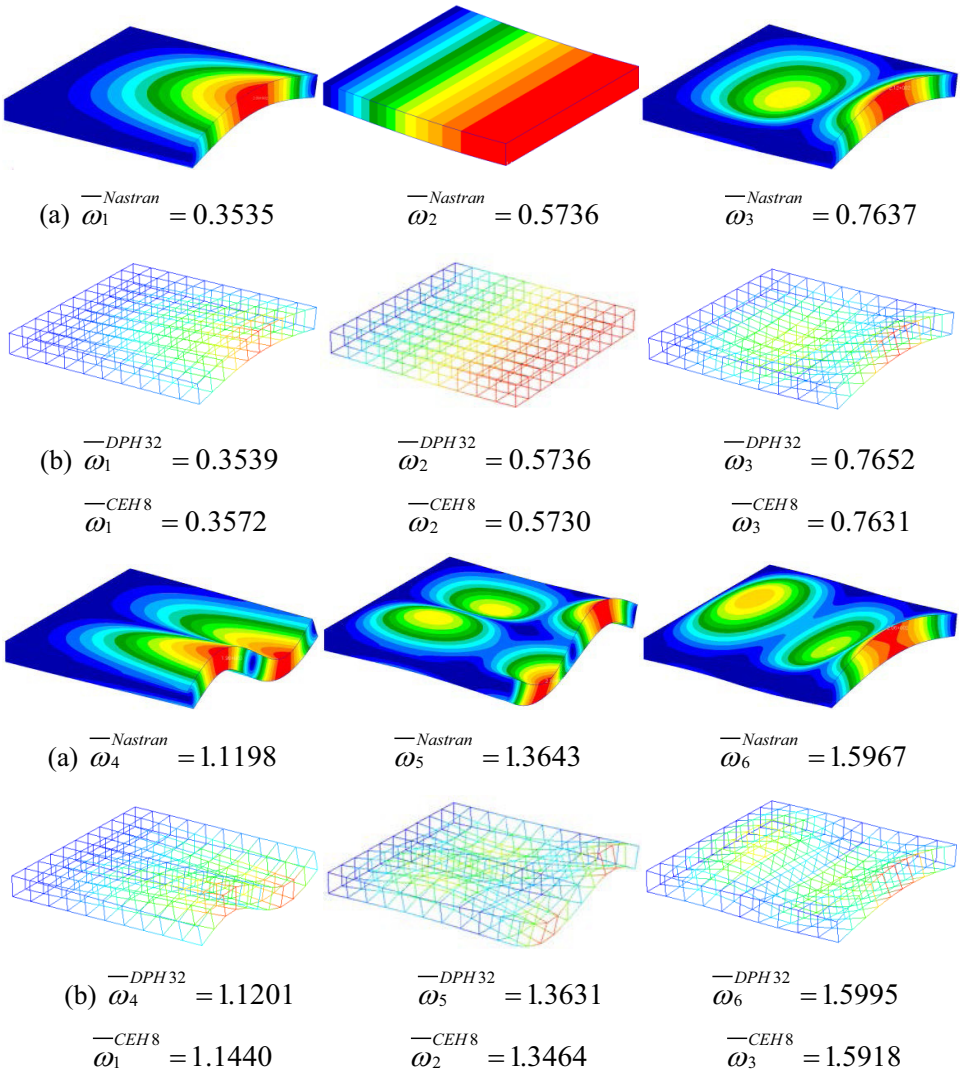

Figure 18: First six non-dimensional frequency parameters and their corresponding mode shapes of a CSFS Square laminated plate by (a) Nastran and (b) present CEH8 and DPH32 elements.

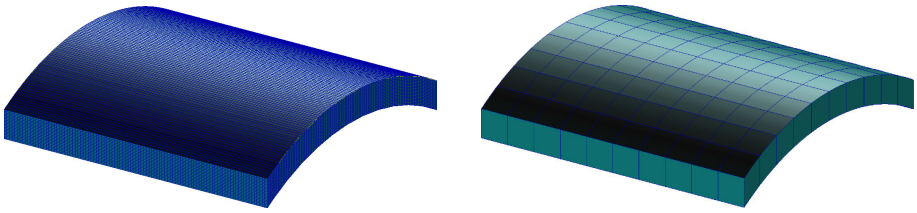

(a) (b)

Figure 19: Finite element model for the 10-ply laminated plate ($a/h = 10$) by (a) Nastran with 400,000 elements and (b) present CEH8 and DPH32 with 100 elements.

3.3 Transient dynamic response of laminated plates

In this section, we study the transient dynamic responses of a simply-supported symmetrical 4-ply ($[0/90]_s$) laminated square plate subjected to a uniform pressure (step load) of magnitude 1kPa at time t= 0. The geometry and material properties are same as the first example. The same CEH8/DPH32 FEM model with a uniform 10×10 mesh is also used to compute the global nodal force vector, mass matrix and stiffness matrix. Newmark beta method is used to evaluate the time-domain numerical integration. Direct transient response by Nastran is also used to obtain the results of displacements, velocities and stresses in each element. The vertical displacements and normal stresses by CEH8/DPH32 elements and by Nastran are presented in Fig. 24–25. It is clearly shown that the results obtained by the present method are in good agreement with numerical results using Nastran. In the meantime, small global matrices derived from the present method significantly improve the computational efficiency. We can further see that the computational accuracy of DPH32 is slightly better than that of CEH8, with a price of slightly higher computational time.

We also consider the same laminated plate subjected to a time-dependent sinusoidal pressure shown in Fig. 26. The problem is solved by present CEH8/DPH32 elements and by Nastran separately. The vertical displacements and normal stresses computed by the present method and by Nastran are presented in Fig. 27–28. Very good agreement is also observed.

4 Conclusion

Through a large number numerical results of static, free vibration, and transient analyses of various laminated plates and shells, it is demonstrated that the proposed CEH8 and DPH32 is capable of accurately and efficiently predicting the static and

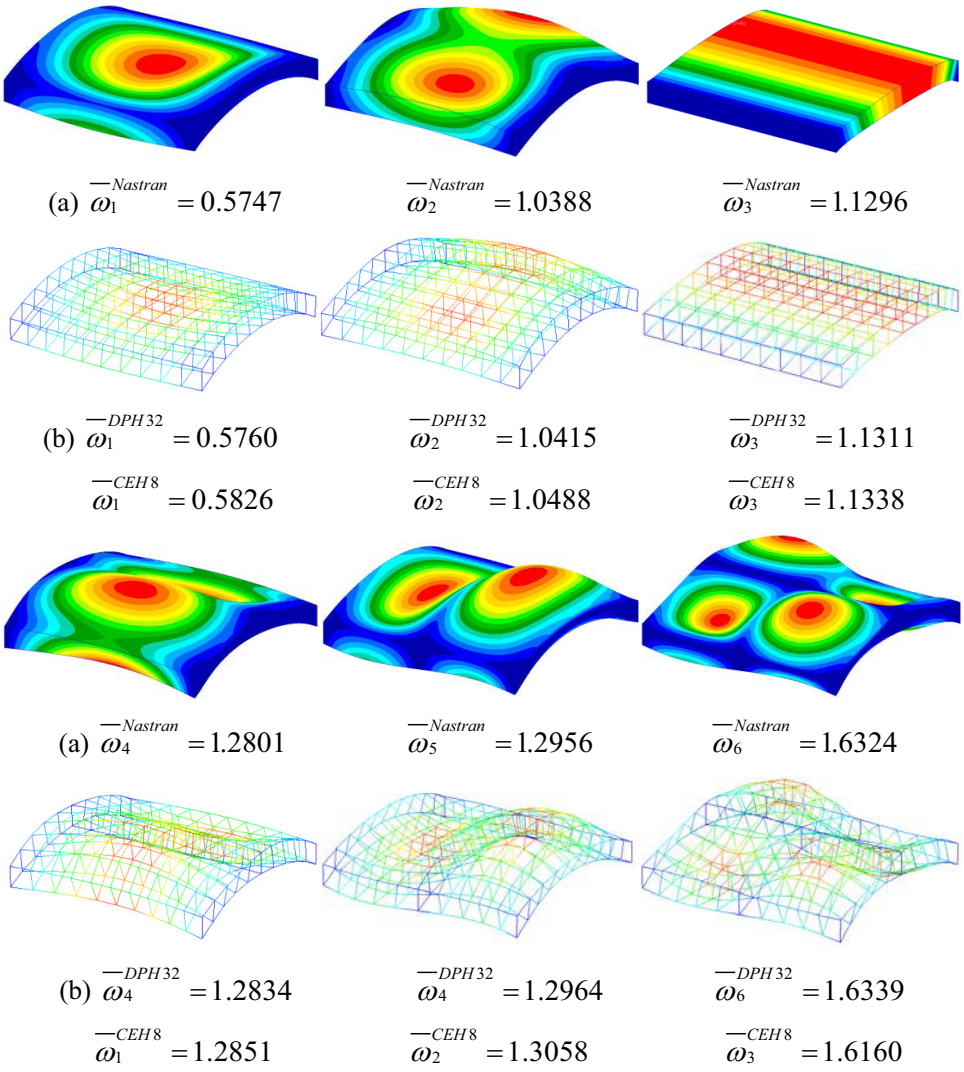

Figure 20: First six non-dimensional frequency parameters and their corresponding mode shapes of a SSSS laminated shell by (a) Nastran and (b) present CEH8 and DPH32 elements.

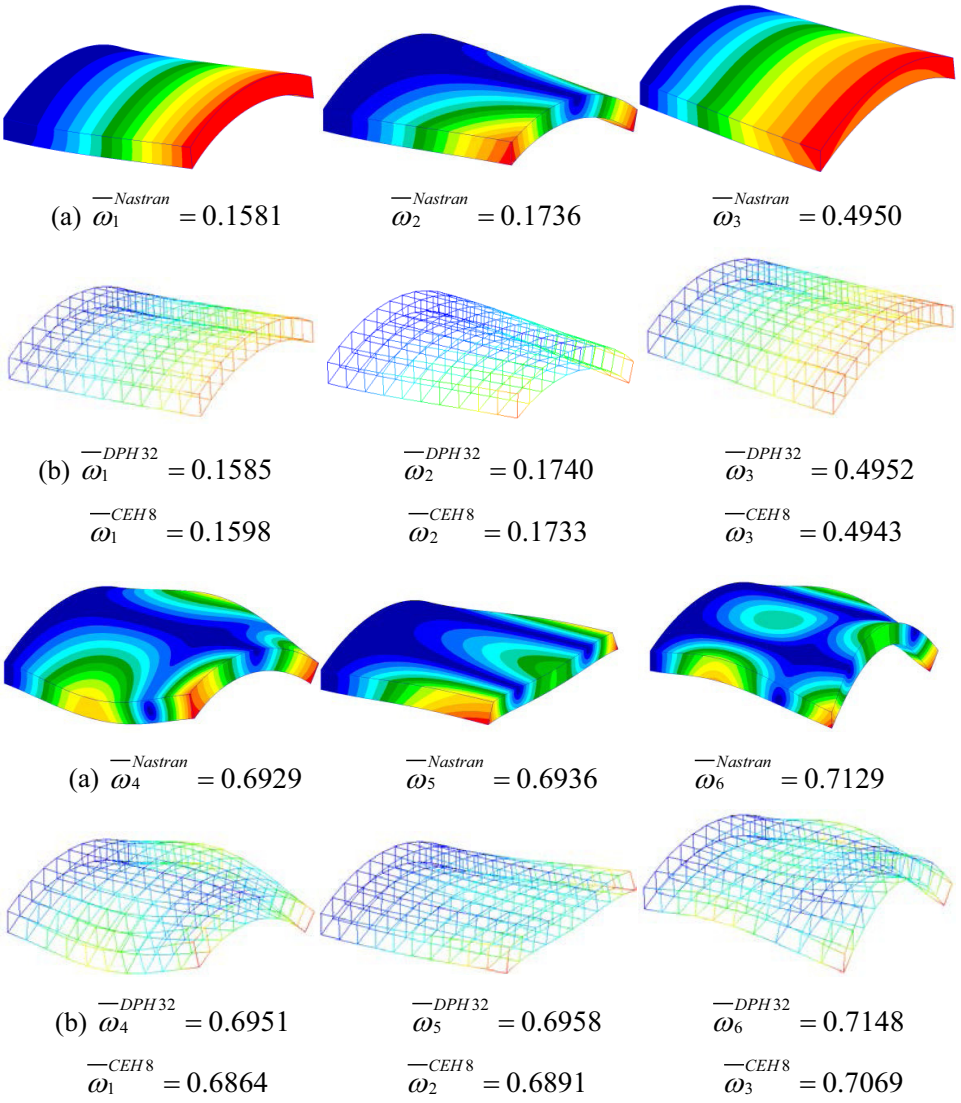

Figure 21: First six non-dimensional frequency parameters and their corresponding mode shapes of a CFFF laminated shell by (a) Nastran and (b) present CEH8 and DPH32 elements.

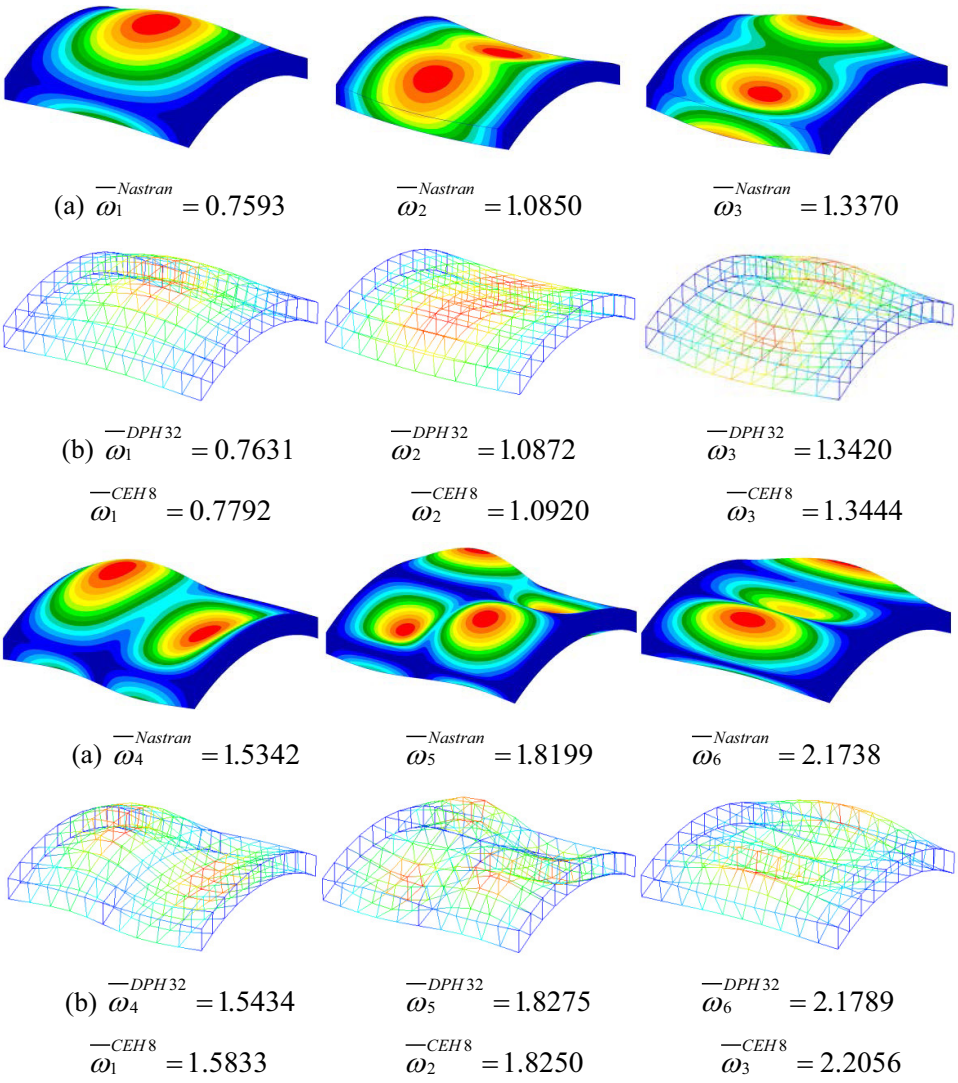

Figure 22: First six non-dimensional frequency parameters and their corresponding mode shapes of a CSCS laminated shell by (a) Nastran and (b) present CEH8 and DPH32 elements.

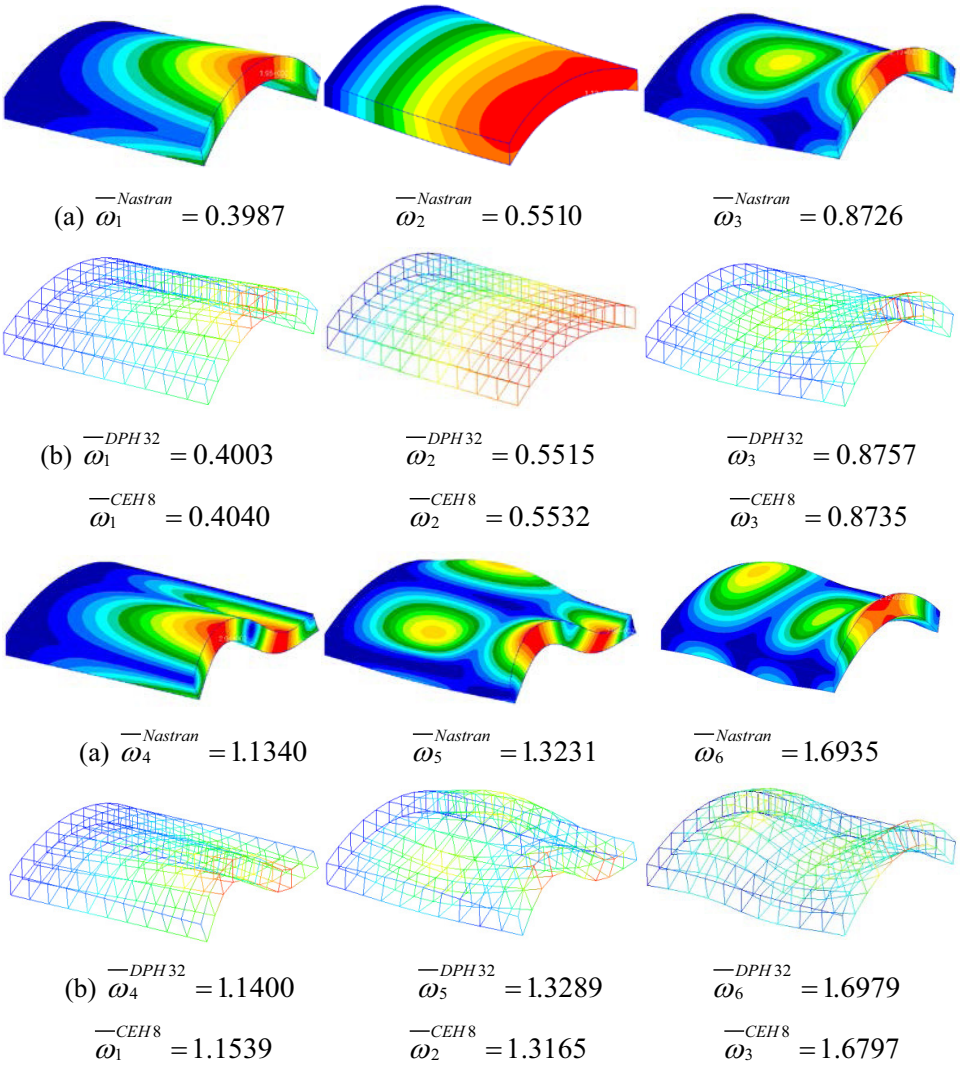

Figure 23: First six non-dimensional frequency parameters and their corresponding mode shapes of a CSFS laminated shell by (a) Nastran and (b) present CEH8 and DPH32 elements.

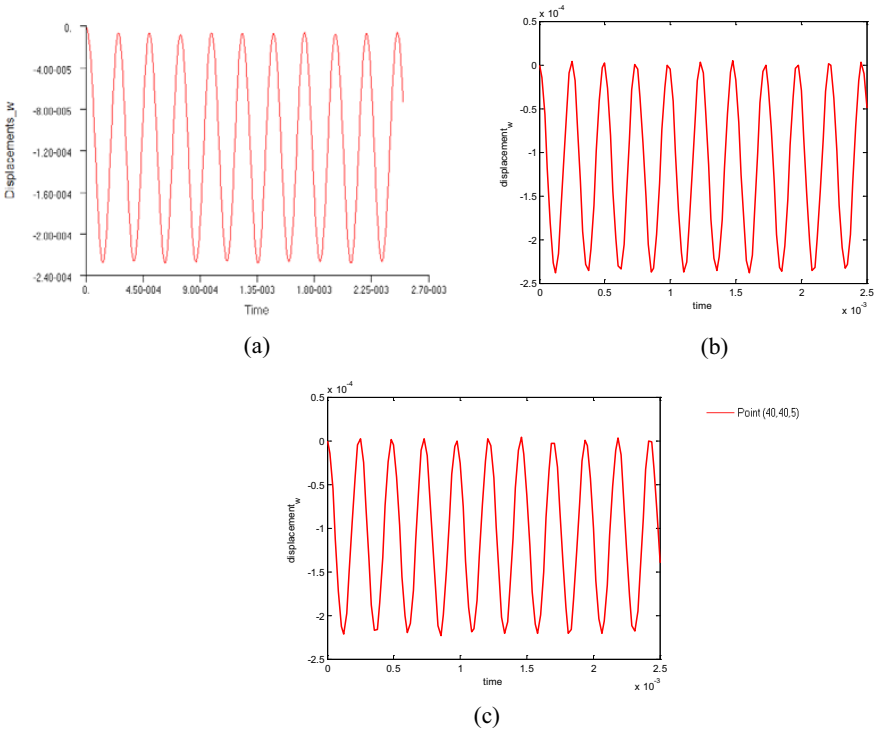

(a) (b) (c)

Figure 24: Vertical displacement response of the laminated plate ($a/h = 10$) by (a) Nastran, (b) DPH32 elements, (c) CEH8 elements

dynamical behaviors of composite laminates in a very simple and cost-effective manner. Because higher-order and layer-wise plate and shell theories involve (1) postulating very complex assumptions of plate/shell kinematics in the thickness direction, (2) defining generalized variables of displacements, strains, and stresses, and (3) developing very complex governing equilibrium, compatibility, and constitutive equations in terms of newly-defined generalized variables, while the currently proposed CEH8 and DPH32 merely involve displacement DOFs at each node, and rely only on the simple theory of solid mechanics, it is thus concluded by the authors that the development of higher-order or layer-wise theories are not entirely necessary for analyses of laminated plates and shells.

Acknowledgement: This research is supported by the Mechanics Section, Vehicle Technology Division, of the US Army Research Labs. The first author acknowledges the financial support by the National High Technology Research and Development Program of China (863 Program, grant No. 2012AA112201). The

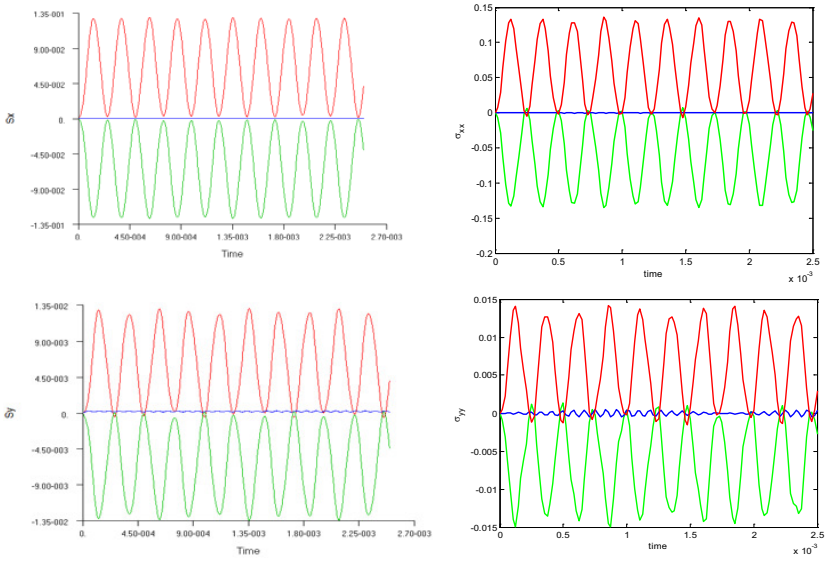

(a) (b)

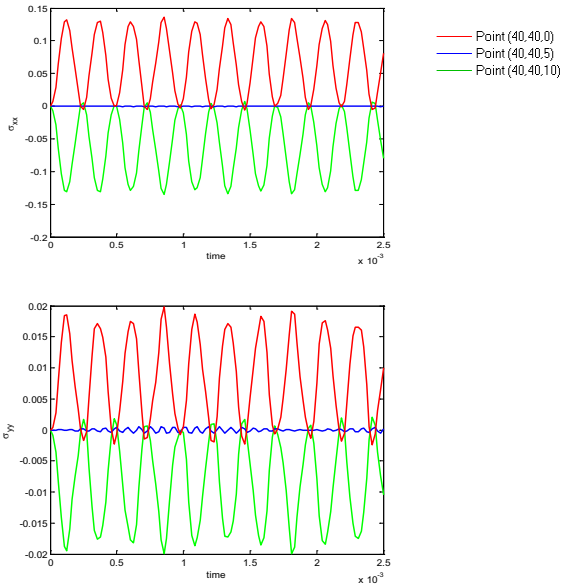

(c)

Figure 25: Normal stress response of the laminated plate ($a/h = 10$) by (a) Nastran, (b) DPH32 elements, (c) CEH8 elements

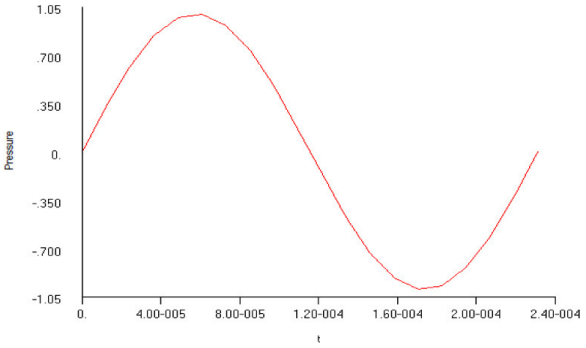

Figure 26: The applied time-dependent sinusoidal pressure

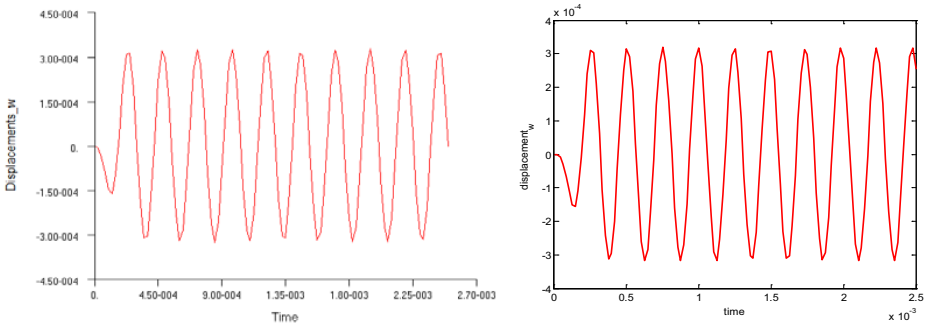

(a) (b)

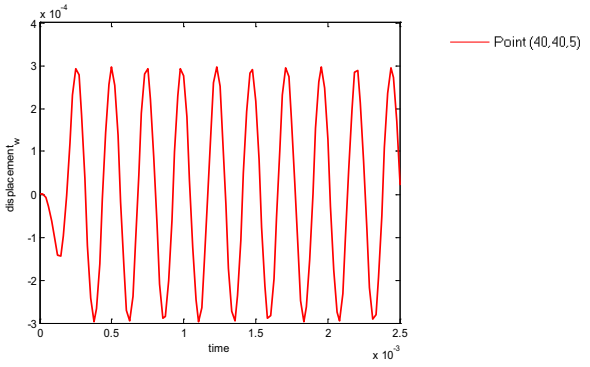

(c)

Figure 27: Vertical displacement response of the laminated plate ($a/h = 10$) by (a) Nastran (b) DPH32 elements, (c) CEH8 elements

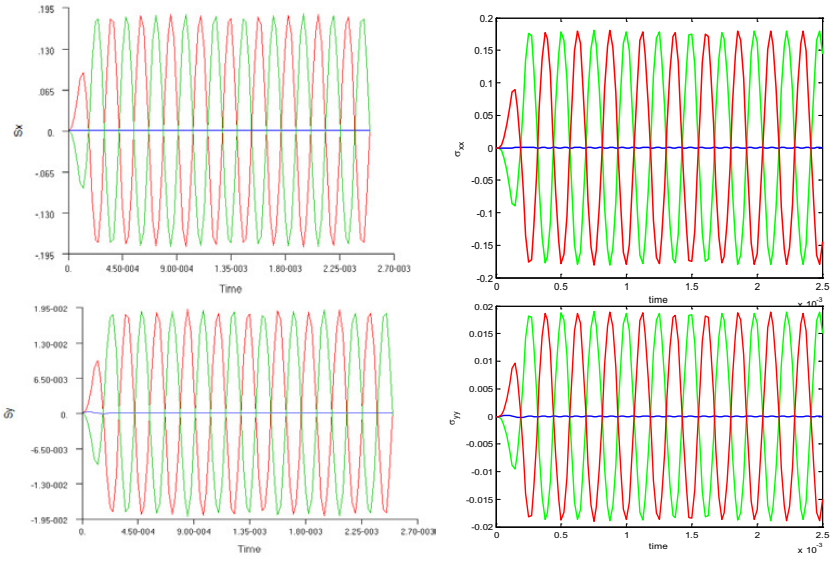

(a) (b)

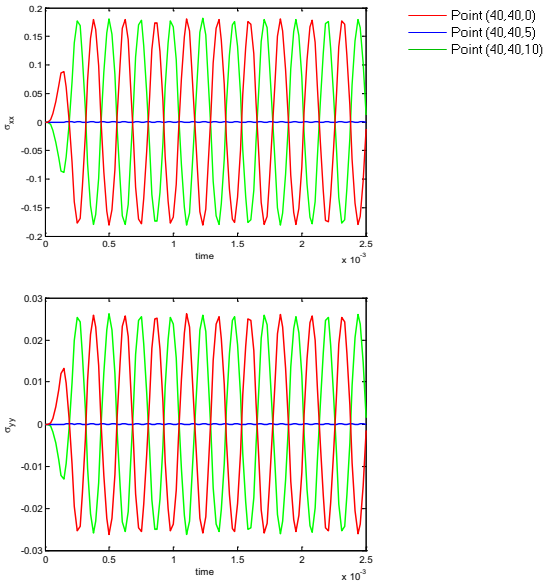

(c)

Figure 28: Normal stress response of the laminated plate ($a/h = 10$) by (a) Nastran, (b) DPH32 elements, (c) CEH8 elements

support of National Natural Science Foundation of China (grant No. 11502069) and Natural Science Foundation of Jiangsu Province (grant No. BK20140838) is also thankfully acknowledged.

References

Atluri, S. N. (2005): *Methods of Computer Modeling in Engineering and the Sciences,* Tech Science Press.

Di Sciuva, M. (1985): Development of an anisotropic, multilayered, shear-deformable rectangular plate element. *Computers & structures*, vol. 21(4), pp. 789-796.

Carrera, E. (2003): Historical review of zig-zag theories for multilayered plates and shells. *Applied Mechanics Reviews*, vol. 56, issue 3, pp. 287-308.

Dong, L.; A.; Atluri, S. N. (2011): A Simple Procedure to Develop Efficient & Stable Hybrid/Mixed Elements, and Voronoi Cell Finite Elements for Macro- & Micromechanics. *CMC: Computers, Materials & Continua*, vol. 24, issue 1, pp. 61-104.

Dong, L.; Alotaibi, A.; Mohiuddine, S. A.; Atluri, S. N. (2014a): Computational methods in engineering: a variety of primal & mixed methods, with global & local interpolations, for well-posed or ill-Posed BCs. *CMES: Computer Modeling in Engineering & Sciences*, vol. 99, no. 1, pp. 1-85.

Dong, L.; El-Gizawy, A. S.; Juhany, K. A.; Atluri, S. N. (2014b): A simple locking-alleviated 4-node mixed-collocation finite element with over-integration, for homogeneous or functionally-graded or thick-section laminated composite beams. *CMC: Computers, Materials & Continua*, vol. 40, issue 1, pp. 49-77.

Dong, L.; El-Gizawy, A. S.; Juhany, K. A.; Atluri, S. N. (2014c): A simple locking-alleviated 3D 8-Node mixed-collocation C^0 finite element with over-integration, for functionally-graded and laminated thick-section plates and shells, with & without z-pins. *CMC: Computers, Materials & Continua*, vol. 41, issue 3, pp. 163-192.

Lo, K. H.; Christensen, R. M.; Wu, E. M. (1977): A high-order theory of plate deformation—part 2: laminated plates. *Journal of Applied Mechanics,* vol. 44, issue 4, pp. 669-676.

Mindlin, R. D. (1951): Influence of rotatory inertia and shear on flexural motions of isotropic, elastic plates. *Journal of Applied Mechanics,* vol. 18, pp. 31-38.

Pandya, B. N.; Kant, T. (1988): Finite element analysis of laminated composite plates using a higher-order displacement model. *Composites Science and Technology*, vol. 32, pp. 137-155.

Ray, R. M.; Dong, L.; Atluri, S. N. (2015): Simple Efficient Smart Finite Elements for the Analysis of Smart Composite Beams. *CMC: Computers, Materials & Continua*, vol. 47, issue 2, pp. 65-99.

Reddy, J. N. (1984): A simple higher-order theory for laminated composite plates. *Journal of Applied Mechanics*, vol. 51, issue 4, pp. 745-752.

Reddy, J. N.; Robbins, D. H. (1994): Theories and computational models for composite laminates. *Applied Mechanics Reviews,* vol. 47, issue 6, pp. 147-169.

Reddy, J. N. (2004): *Mechanics of laminated composite plates and shells: theory and analysis*, CRC press.

Reissner, E. (1945): The effect of transverse shear deformation on the bending of elastic plates. *Journal of Applied Mechanics,* vol. 12, pp. 69-77.

Swift, G. W.; Heller, R. A. (1974): Layered beam analysis. *Journal of the Engineering Mechanics Division*, vol. 100, issue 2, pp. 267-282.

Seide, P. (1980): An improved approximate theory for the bending of laminated plates. *Mechanics today*, vol. 5, pp. 451-465.

Timoshenko, S.; Woinowsky-Krieger, S. (1959): *Theory of Plates and Shells.* McGraw hill, New York.

Zienkiewicz, O. C.; Taylor, R. L. (1977): *The finite element method (Vol. 3).* London: McGraw-hill.